23

Discrete-Time Dynamic Image-Segmentation System

Ken'ichi Fujimoto, Mio Kobayashi and Tetsuya Yoshinaga
The University of Tokushima
Japan

1. Introduction

The modeling of oscillators and their dynamics has interested researchers in many fields such as those in physics, chemistry, engineering, and biology. The Hodgkin-Huxley (Hodgkin & Huxley, 1952) and Fitzhugh-Nagumo models (FitzHugh, 1961), which corresponds to the Bonhöffer van der Pol (BvP) equation, are well-known models of biological neurons. They have been described by differential equations, i.e., they are continuous-time relaxation oscillators. Discrete-time oscillators, e.g., one consisting of a recurrent neural network (Haschke & Steil, 2005) and another consisting of a spiking neuron model (Rulkov, 2002), have been proposed.

Synchronization observed in coupled oscillators has been established to be an important topic (Pikovsky et al., 2003; Waller & Kapral, 1984). Research on coupled oscillators has involved studies on pattern formation (Kapral, 1985; Oppo & Kapral, 1986), image segmentation (Shareef et al., 1999; Terman & Wang, 1995; Wang & Terman, 1995; 1997), and scene analysis (Wang, 2005). Of these, a locally excitatory globally inhibitory oscillator network (LEGION) (Wang & Terman, 1995), which is a continuous-time dynamical system, has been spotlighted as an ingenious image-segmentation system. A LEGION can segment an image and exhibit segmented images in a time series, i.e., it can spatially and temporally segment an image. We call such processing dynamic image segmentation. A LEGION consists of relaxation oscillators arranged in a two-dimensional (2D) grid and an inhibitor globally connected to all oscillators and it can segment images according to the synchronization of locally coupled oscillators. Image segmentation is the task of segmenting a given image so that homogeneous image blocks are disjoined; it is a fundamental technique in computer vision, e.g., object recognition for a computer-aided diagnosis system (Doi, 2007) in medical imaging. The problem with image segmentation is still serious, and various frameworks have been proposed (Pal & Pal, 1993; Suri et al., 2005) to solve this.

We proposed a discrete-time oscillator model consisting of a neuron (Fujimoto et al., 2008), which was modified from a chaotic neuron model (Aihara, 1990; Aihara et al., 1990), coupled with an inhibitor. Despite discrete-time dynamics as well as the recurrent neural network (Haschke & Steil, 2005), a neuron in our oscillator can generate a similar oscillatory response formed by a periodic point to an oscillation as observed in a continuous-time relaxation oscillator model, e.g., the BvP equation. This is a key attribute in our idea. Moreover, we proposed a neuronal network system consisting of our neurons (discrete-time oscillators) arranged in a 2D grid and an inhibitor globally coupled to all neurons. As well as

a LEGION, our neuronal network system can work as a dynamic image-segmentation system according to the oscillatory responses of neurons. Our system provides much faster dynamic image segmentation than a LEGION on a digital computer because numerical integration is not required (Fujimoto et al., 2008). Another advantage of our system is that it simplifies the investigation of bifurcations of fixed points and periodic points due to the discrete-time dynamical system. A fixed point and a periodic point correspond to non-oscillatory and periodic oscillatory responses. Knowledge on the bifurcations of responses allows us to directly design appropriate system parameters to dynamically segment images. The assigned system parameters are made available by implementing our dynamic image-segmentation system into hardware such as field-programmable gate array devices (Fujimoto et al., 2011b). This article describes the derivation of a model reduced from our dynamic image-segmentation system that can simplify bifurcation analysis. We also explain our method of bifurcation analysis based on dynamical systems theory. Through analysis in reduced models with two or three neurons using our method of analysis, we find parameter regions where a fixed point or a periodic point exists. We also demonstrate that our dynamic image-segmentation system, whose system parameters were appropriately assigned according to the analyzed results, can work for images with two or three image regions. To demonstrate that segmentation is not limited to three in the system, we also present a successive algorithm for segmenting an image with an arbitrary number of image regions using our dynamic image-segmentation system.

2. Discrete-time dynamic image-segmentation system

2.1 Single neuronal system

Figure 1(a) illustrates the architecture of a system consisting of a neuron (Fujimoto et al., 2008) and an inhibitor. Here, let us call it a single neuronal system. Our neuron model modified from a chaotic neuron model (Aihara, 1990; Aihara et al., 1990) has two internal state variables, x and y; z corresponds to the internal state variable of an inhibitor, in which $x, y, z \in \mathbb{R}$ with $\mathbb{R}$ denoting the set of real numbers. Let the sum of internal state values in a neuron, i.e. $x + y$, be the activity level of a neuron. The dynamics of the single neuronal system is described by difference equations:

$$x(t+1) = k_f x(t) + d + W_x \cdot g(x(t) + y(t), \theta_c) - W_z \cdot g(z(t), \theta_z) \tag{1a}$$

$$y(t+1) = k_r y(t) - \alpha \cdot g(x(t) + y(t), \theta_c) + a \tag{1b}$$

$$z(t+1) = \phi \left\{ g\left(g(x(t) + y(t), \theta_f), \theta_d \right) - z(t) \right\}. \tag{1c}$$

The $t \in \mathbb{Z}$ denotes the discrete time where $\mathbb{Z}$ expresses the set of integers. $g(\cdot, \cdot)$ is the output function of a neuron or an inhibitor and is described as

$$g(u(t), \theta) = \frac{1}{1 + \exp(-(u(t) - \theta)/\varepsilon)}. \tag{2}$$

Note that $g(\cdot, \theta_d)$ where $g(x(t) + y(t), \theta_f)$ is nested in Eq. (1c) is neither output function, but a function to find the firing of a neuron that corresponds to a high level of activity. Therefore, an inhibitor plays roles in detecting a fired neuron and suppressing the activity level of a neuron at the next discrete time. The k_f, k_r, and ϕ are coefficients corresponding to the gradient of x, y, and z. The d denotes an external direct-current (DC) input. The W_x and α are self-feedback gains in a neuron, and W_z is the coupling coefficient from an inhibitor to a neuron. The a is a

bias term in a neuron. The θ_c and θ_z are threshold parameters in output functions of a neuron and an inhibitor, respectively. Also, θ_f and θ_d are threshold parameters to define the firing of a neuron and to detect a fired neuron, respectively. The ε is a parameter that determines the gradient of the sigmoid function (2) at $u(t) = \theta$.

When we set all the parameters to certain values, our neuron can generate a similar oscillatory response formed by a periodic point to an oscillation as observed in a continuous-time relaxation oscillator model. For instance, the time evolution of a generated response, in which this is a waveform, is shown in Fig. 1(b) for initial values, $(x(0), y(0), z(0)) = (32.108, -31.626, 0.222)$, at $k_f = 0.5$, $d = 2$, $W_x = 15$, $\theta_c = 0$, $W_z = 15$, $\theta_z = 0.5$, $k_r = 0.89$, $\alpha = 4$, $a = 0.5$, $\phi = 0.8$, $\theta_f = 15$, $\theta_d = 0$, and $\varepsilon = 0.1$. To clarify the effect of the inhibitor, we have shown the activity level of the neuron and the internal state of the inhibitor on the vertical axis in this figure. The points marked with open circles "$\circ$" indicate the values of $x + y$ and z at discrete time t. Although the response of a neuron or an inhibitor is formed by a series of points because of its discrete-time dynamics, we drew lines between temporally adjacent points as a visual aid. Therefore, our neuron coupled with an inhibitor is available as a discrete-time oscillator.

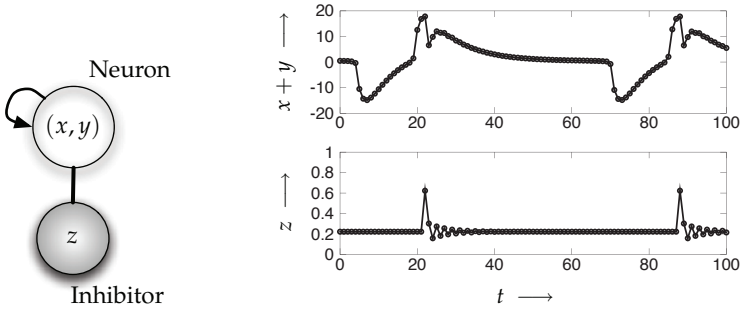

(a) Architecture (b) Oscillatory response

Fig. 1. Architecture of single neuronal system and generated oscillatory response

2.2 Neuronal network system

We have proposed a neuronal network system for dynamic image segmentation (Fujimoto et al., 2008). Figure 2(a) outlines the architecture of our system for a 2D image with P pixels. It is composed of our neurons that have as many pixels as in a given image and an inhibitor that is called a global inhibitor because it is connected with all neurons. All neurons are arranged in a 2D grid so that one corresponds to a pixel, and a neuron can have excitatory connections to its neighboring neurons. Here, we assumed that a neuron could connect to its four-neighboring ones. The formation of local connections between neighboring neurons is determined according to the value of DC input to each neuron. Note that, we can use our neuronal network system, in which neurons are arranged in a 3D grid so that one neuron corresponds to a voxel, which means a volumetric picture element, as a dynamic image-segmentation system for a 3D image.

The architecture for the ith neuron in a neuronal network system is illustrated in Fig. 2(b). The open and closed circles at the ends of the arrows correspond to excitatory and inhibitory

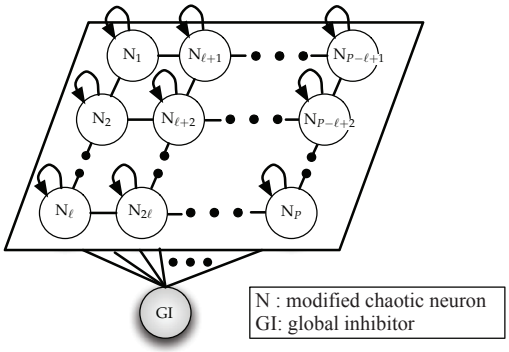

(a) Neuronal network system

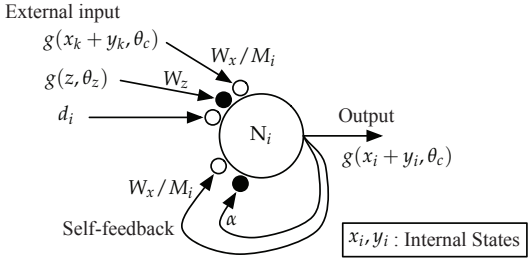

(b) The ith neuron

Fig. 2. Architecture of neuronal network system and a neuron

couplings. A neuron can receive external inputs from neighboring ones connected to it. An external input from another neuron can induce in-phase synchronization in the responses of connected neurons. Note that the number of external inputs in Fig. 2(b) indexed by $g(x_k + y_k, \theta_c)$ is the same as that of the other neurons connected to the ith neuron; moreover, when the DC-input value to the ith neuron is low, positive self-feedback vanishes and the neuron also has no connection to the others. W_x/M_i and W_z in external inputs represent coupling weights; the other W_x/M_i and α are feedback gains, where M_i denotes the number of connections to the ith neuron and neighboring neurons. What M_i means will be explained later.
The dynamics of our neuronal network system is described as

$$x_i(t+1) = k_f x_i(t) + d_i + \sum_{k \in L_i} \frac{W_x}{M_i} g(x_k(t) + y_k(t), \theta_c) - W_z \cdot g(z(t), \theta_z) \tag{3a}$$

$$y_i(t+1) = k_r y_i(t) - \alpha \cdot g(x_i(t) + y_i(t), \theta_c) + a \tag{3b}$$

$$(i = 1, 2, \ldots, P)$$

$$z(t+1) = \phi \left\{ g\left(\sum_{n=1}^{P} g(x_n(t) + y_n(t), \theta_f), \theta_d \right) - z(t) \right\}. \tag{3c}$$

The $g(\cdot,\cdot)$ was already defined in Eq. (2). The third term on the right hand side of Eq. (3a) denotes the ith neuron's self-feedback and external inputs from neighboring neurons, in which L_i represents an index set for neurons connected to the ith one. Therefore, the maximum number of elements in L_i is five in the architecture in Fig. 2(a). The M_i expresses the number of elements in L_i. Note that, when the ith neuron has no connection to neighboring neurons including itself, i.e., $M_i = 0$, we treat it as $W_x / M_i = 0$ because division by zero occurs.
As seen in Eq. (3c), the dynamics of a global inhibitor is improved from that in Eq. (1c) so that it can detect one or more firing neurons; moreover, it suppresses the activity levels of all neurons via negative couplings described at the fourth term in the right hand side of Eq. (3a). Therefore, when we set all the parameter values in Eq. (3) to those described in Sec. 2.1, only neurons with self-feedback can generate oscillatory responses.

2.3 Scheme of dynamic image segmentation

There is an image segmentation scheme using our neuronal network system in Fig. 3. For simplicity, let us now consider a simple gray-level image with 3×3 pixels. The image contains two image regions consisting of the same gray-level pixels: the first is composed of the first and fourth pixels, and the second is made up of only the ninth pixel.
Nine neurons are arranged in a 3×3 grid for the given image. The value of DC input, d_i, is associated with the gray level of the ith pixels. A neuron with a high DC-input value forms positive self-feedback and also connects to neighboring ones with similar DC-input values. Therefore, the red and blue neurons in this schematic have positive self-feedback connections and can generate oscillatory responses; the others corresponding to black pixels have no self-feedback and do not fire. Direct connection is formed between the red neurons because they correspond to pixels with the same gray levels, i.e., they have the same DC-input values. As seen from the red waveforms in Fig. 3, direct connection induces in-phase synchronization in the responses of coupled neurons. However, as seen from the red and blue waveforms, the responses of uncoupled neurons corresponding to pixels in different image regions are out of phase. This effect is produced by the global inhibitor that detects one or more firing neurons and suppresses the activity levels of all neurons with its own kindling. By assigning

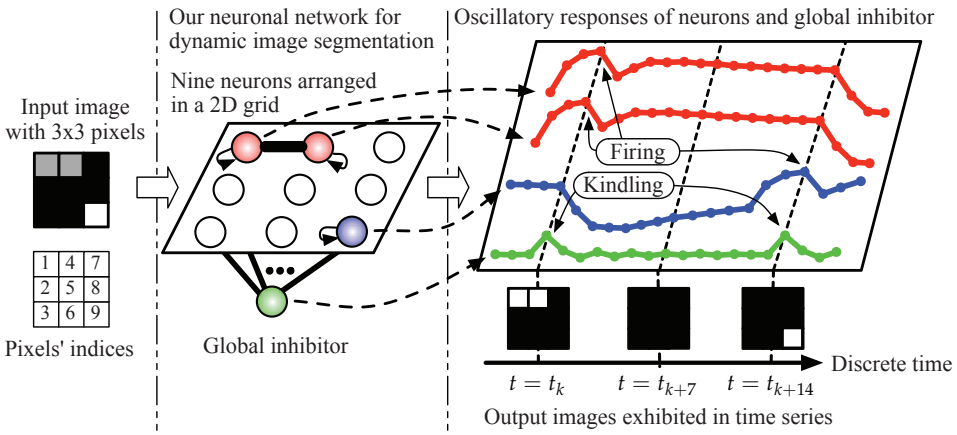

Fig. 3. Scheme of dynamic image segmentation using our system

the ith pixel value in the output image at time t to a high value corresponding to the white pixel only if $x_i(t) + y_i(t) \geq \theta_f$, segmented images are output and are exhibited in a time series. As a result, the given image is spatially and temporally segmented, i.e., dynamic image segmentation is achieved.

3. Analysis for parameter design

3.1 Reduced model

Our neuronal network model has complex dynamics and a variety of nonlinear phenomena such as synchronized neuron responses and bifurcations in these responses are therefore expected to occur in our system. From the viewpoint of dynamical systems theory, detailed analyses of the local and global bifurcations observed in our system would be interesting. However, we have only concentrated on analysis to design appropriate parameter values for dynamic image segmentation in this article, i.e., to find parameter regions where there are stable non-oscillatory or periodic oscillatory responses.

First, we need to derive a reduced model to simplify bifurcation analysis. Let us consider a dynamic image-segmentation system for a P-pixel image with Q image regions, where generally $Q \ll P$. A reduced model consists of a global inhibitor and Q neurons without direct coupling to the others as illustrated in Fig. 4. Here, we call it a Q-coupled system. A neuron in a Q-coupled system stands for neurons corresponding to all pixels in the same image region in our original neuronal system in Fig. 2(a). This reduced model is derived from three assumptions (Fujimoto et al., 2009b) in our dynamic image segmentation system for an image with Q image regions: 1) all pixel values in an identical image region are the same; viz., all neurons corresponding to pixels in an image region have the same DC-input values and are locally coupled with one another, 2) the responses of all neurons corresponding to pixels in an identical image region are synchronized in phase; this arises naturally from the first assumption, and 3) connections from the global inhibitor to the neurons are negligible because neurons corresponding to pixels with low gray-levels do not fire.

A non-oscillatory response and a periodic oscillatory response correspond to a fixed point and a periodic point. Therefore, knowing about their bifurcations in a Q-coupled system allows us to directly design appropriate parameter values to dynamically segment any sized image with Q image regions.

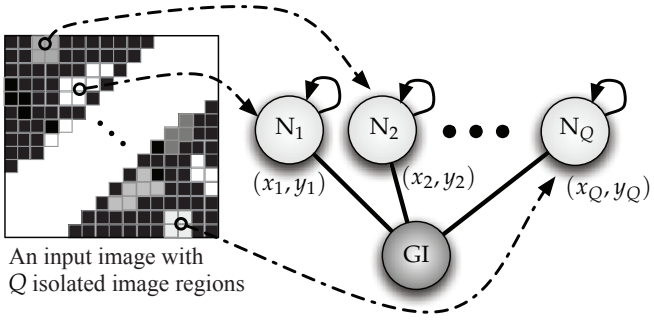

Fig. 4. Architecture of Q-coupled system and its correspondence to image with Q image regions

Now, let $\boldsymbol{x}(t) = (x_1(t), y_1(t), \ldots, x_Q(t), y_Q(t), z(t))^\top \in \mathbb{R}^V$, where $\top$ denotes the transpose of a vector. The dynamics of the Q-coupled system is described by a V-dimensional discrete-time dynamical system where $V = 2Q + 1$ as

$$\boldsymbol{x}(t+1) = \boldsymbol{f}(\boldsymbol{x}(t)), \tag{4}$$

or equivalently, an iterated map defined by

$$\boldsymbol{f} : \mathbb{R}^V \to \mathbb{R}^V; \boldsymbol{x} \mapsto \boldsymbol{f}(\boldsymbol{x}). \tag{5}$$

The nonlinear function, $\boldsymbol{f}$, describes the dynamics of the Q-coupled system given by

$$\boldsymbol{f}\begin{pmatrix} x_1 \\ y_1 \\ \vdots \\ x_Q \\ y_Q \\ z \end{pmatrix} = \begin{pmatrix} k_f x_1 + d_1 + W_x \cdot g(x_1 + y_1, \theta_c) - W_z \cdot g(z, \theta_z) \\ k_r y_1 - \alpha \cdot g(x_1 + y_1, \theta_c) + a \\ \vdots \\ k_f x_Q + d_Q + W_x \cdot g(x_Q + y_Q, \theta_c) - W_z \cdot g(z, \theta_z) \\ k_r y_Q - \alpha \cdot g(x_Q + y_Q, \theta_c) + a \\ \phi\left\{ g\left(\sum_{n=1}^{Q} g(x_n + y_n, \theta_f), \theta_d \right) - z \right\} \end{pmatrix} \tag{6}$$

where $g(\cdot, \cdot)$ was defined in Eq. (2).

3.2 Method of bifurcation analysis

A non-oscillatory response observed in the Q-coupled system corresponds to a fixed point of $\boldsymbol{f}$ in Eq. (5), and a periodic oscillatory response is formed by a periodic point of $\boldsymbol{f}$. Therefore, we can find their local bifurcations for the change in a system parameter value using a method of analysis based on qualitative bifurcation theory for discrete-time dynamical systems. The results from analyzing bifurcation in a reduced model enabled us to design suitable parameter values in our neuronal network system for dynamic image segmentation.

The following explains our method of analysis. Let us now consider a point, $\boldsymbol{x}^*$, satisfying

$$\boldsymbol{x}^* - \boldsymbol{f}(\boldsymbol{x}^*) = \boldsymbol{0}. \tag{7}$$

This is called a fixed point of $\boldsymbol{f}$ in Eq. (5) and corresponds to a non-oscillatory response observed in the Q-coupled system. The characteristic equation of $\boldsymbol{x}^*$ is defined as

$$\det\left(\mu \boldsymbol{E} - D\boldsymbol{f}(\boldsymbol{x}^*)\right) = 0, \tag{8}$$

where $\boldsymbol{E}$ and $D\boldsymbol{f}(\boldsymbol{x}^*)$ correspond to the $V \times V$ identity matrix and the Jacobian matrix of $\boldsymbol{f}$ at $\boldsymbol{x} = \boldsymbol{x}^*$. Moreover, the roots of Eq. (8), i.e., characteristic multipliers, are described as

$$\{\mu_1, \mu_2, \ldots, \mu_V\} = \left\{ \mu_i \in \mathbb{C} \;\middle|\; \det\left(\mu \boldsymbol{E} - D\boldsymbol{f}(\boldsymbol{x}^*)\right) = 0 \right\}, \tag{9}$$

where $\mathbb{C}$ denotes the set of complex numbers. When the values of all $|\mu_i|$s are neither unity nor zero, we say that $\boldsymbol{x}^*$ is hyperbolic. Now, let us assume $\boldsymbol{x}^*$ is a hyperbolic fixed point. Let $\boldsymbol{U}$ be the intersection of $\mathbb{R}^V$ and the direct sum of the generalized eigenspaces of $D\boldsymbol{f}(\boldsymbol{x}^*)$ such that $|\mu_i| > 1, \forall i$; $\boldsymbol{U}$ is called the unstable subspace of $\mathbb{R}^V$. Moreover, let $\boldsymbol{H} = D\boldsymbol{f}(\boldsymbol{x}^*)|_{\boldsymbol{U}}$. The topological type of a hyperbolic fixed point is classified according to the value of $\dim \boldsymbol{U}$ and the sign of $\det \boldsymbol{H}$ (Kawakami, 1984).

A hyperbolic fixed point bifurcates when its stability is varied, or more correctly its topological type is changed, according to variations in a system parameter value; change in a topological type occurs when one or more characteristic multipliers are on the unit circle in the complex plane. There are generally three types of co-dimension-one bifurcations, i.e., tangent (saddle-node), period-doubling, and Neimark-Sacker bifurcations. D-type of branching (pitchfork bifurcation) can also appear as a degenerate case of tangent bifurcation in only a dynamical system that is symmetrical. Tangent bifurcation or D-type of branching appears if $\mu = +1$, period-doubling bifurcation occurs when $\mu = -1$, and Neimark-Sacker bifurcation is generated when $\mu = e^{j\varphi}$, where $j = \sqrt{-1}$ except for $\mu = \pm 1$.
A bifurcation point of $\boldsymbol{x}^*$ is computed by solving simultaneous equations consisting of Eqs. (7) and (8) as the values of $\boldsymbol{x}^*$ and a system parameter are unknown; we employed Newton's method for the numerical determination. The Jacobian matrix of the simultaneous equations used in Newton's method is derived from the first and second derivatives of $\boldsymbol{f}$. Note that, in Eq. (7), a fixed point, $\boldsymbol{x}^*$, becomes an m-periodic point by replacing $\boldsymbol{f}$ with $\boldsymbol{f}^m$, which denotes the m-times iteration of $\boldsymbol{f}$, where m is a natural number such that $m \geq 2$. We can define an m-periodic point and its bifurcations according to $\boldsymbol{f}^m$; moreover, we can numerically compute the bifurcation points of an m-periodic point as well as those of a fixed point.
As previously mentioned, we focused on bifurcation analysis to design suitable parameter values for our dynamic image segmentation system. Therefore, we will next illustrate parameter regions where there are stable fixed or stable periodic points in two-parameter bifurcation diagrams.

3.3 Results of analysis

We will now illustrate parameter regions where there are stable fixed or periodic points with our method of analyzing bifurcations. Knowing about the bifurcations allows us to directly set system-parameter values that yield successful results for dynamic image segmentation.
We treated a single neuronal system and two- and three-coupled systems and set the system parameter values in Eqs. (2) and (6) except for k_r, ϕ, and d_is to $\varepsilon = 0.1$, $k_f = 0.5$, $W_x = 15$, $\theta_c = 0$, $W_z = 15$, $\theta_z = 0.5$, $\alpha = 4$, $a = 0.5$, $\theta_f = 15$, and $\theta_d = 0$. In the bifurcation diagrams that follow, we used symbols G_ℓ^m, I_ℓ^m, NS_ℓ^m, and D_ℓ^m to denote tangent, period-doubling, and Neimark-Sacker bifurcations, and D-type of branching for an m-periodic point. The subscript series number ℓ was appended to distinguish bifurcation sets of the same type for an m-periodic point. Note that these symbols indicate bifurcations of a fixed point if $m = 1$.

3.3.1 Single neuronal system

This is the reduced model of a dynamic image segmentation system for an image with only one image region. Its architecture is outlined in Fig. 1(a). It may seem that the analysis of bifurcations observed in this reduced model is meaningless for dynamic image segmentation. However, the existence of a fixed point in this model leads to considerable knowledge to devise an algorithm for dynamic image segmentation as will be explained later.
We set $d = 2$ and used k_r and ϕ as unfixed parameters to analyze bifurcation. As shown in Fig. 1(b), an oscillatory response was observed in this model with $k_r = 0.89$ and $\phi = 0.8$. Moreover, we found a stable fixed point, $\boldsymbol{x}^* = (32.244, -23.333, 0.22222)$, at k_r = 0.85 and ϕ = 0.8. We investigated a parameter region where there was a stable fixed point and also found the genesis of the oscillatory response (Fujimoto et al., 2009b).
Figure 5 shows a two-parameter bifurcation diagram on a fixed point in the (k_r, ϕ)-plane. We found three Neimark-Sacker bifurcation sets and located the shaded parameter region where

there was a stable fixed point. When we gradually changed the value of k_r under $\phi = 0.8$ so that the parameter point passed through the bifurcation line indexed by NS_1^1 from the shaded region to the non-shaded region, the stable fixed point destabilized on the Neimark-Sacker bifurcation line. As a result, an oscillatory response was generated as seen in Fig. 6. In the numerical simulation, we set $k_r = 0.88975$ and $\phi = 0.8$ that correspond to the parameter point in the neighborhood at right of NS_1^1 in Fig. 5; the initial values were set to $\boldsymbol{x}(0) = (32.10, -31.58, 0.2222)$, which is in the vicinity of the destabilized fixed point. That is, this figure gives the time evolution in the transient state that starts from the destabilized fixed point to generate an oscillatory response. Although we observed an oscillatory response in the other non-shaded region surrounded by NS_2^1 and NS_3^1, it is not suited to dynamic image segmentation because of its small amplitude and short period.

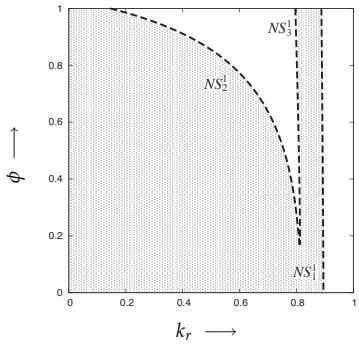

Fig. 5. Bifurcations of fixed point observed in single neuronal system

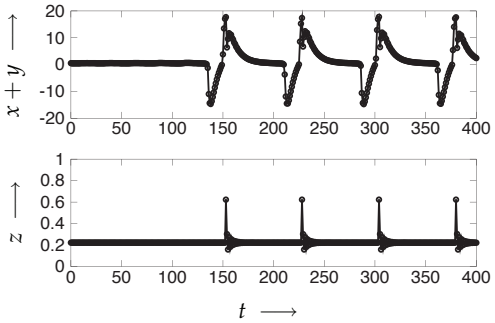

Fig. 6. Oscillatory response caused by Neimark-Sacker bifurcation of stable fixed point

3.3.2 Two-coupled system

This two-coupled system consists of a global inhibitor and two neurons without direct coupling to other neuron. This was derived as a reduced model of our scheme to dynamically segment an image with two image regions.

Here, the unfixed parameters were set to $d_1 = d_2 = 2$, which means that all pixel values in the two image regions are the same. Therefore, this system is symmetrical for the exchange of

(x_1, y_1) and (x_2, y_2) from Eq. (6) at $d_1 = d_2$. The k_r and ϕ were used as unfixed parameters in the analysis of bifurcation that is discussed below.

First, we investigated the bifurcations of a fixed point in a symmetrical two-coupled system (Fujimoto et al., 2009b) where we observed a stable fixed point, $\boldsymbol{x}^* = (32.244, 32.244, -23.333, -23.333, 0.222)$, at $k_r = 0.85$ and $\phi = 0.8$. The occurrence of a fixed point is adverse for dynamic image segmentation because only black images are output; this means dynamic image segmentation has failed. By analyzing bifurcation for the fixed point, we obtained the two-parameter bifurcation diagram in Fig. 5, i.e., this is the same as that for the results obtained for the fixed point in the single neuronal system.

We observed two types of oscillatory responses formed by periodic points at $k_r = 0.89$ and $\phi = 0.8$. Figure 7 shows in-phase and out-of-phase oscillatory responses in which the blue and red points correspond to the responses of the first and second neurons. To understand their phases better, we also drew phase portraits.

Figure 8(a) illustrates bifurcation sets of several in-phase periodic points, and the line marked NS_1^1 at the bottom left corresponds to the Neimark-Sacker bifurcation set of the fixed point. As seen in the figure, we found the tangent bifurcations of in-phase periodic points. There is a stable in-phase m-periodic point in the shaded parameter region surrounded by G_1^m and G_2^m for $m = 60, 61, \ldots, 70$. Therefore, in-phase periodic points could be observed in the shaded parameter regions in the right parameter regions of NS_1^1. Note that in-phase periodic points

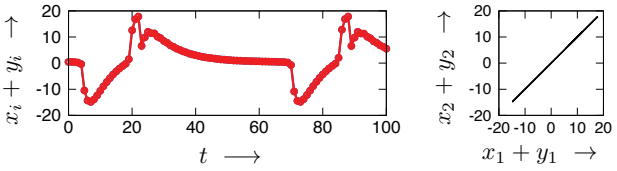

(a) In-phase oscillatory response

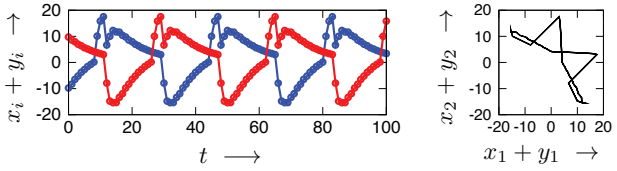

(b) Out-of-phase oscillatory response

Fig. 7. Different types of oscillatory responses observed in symmetric two-coupled system at $k_r = 0.89$ and $\phi = 0.8$

are inappropriate for dynamically segmenting an image with two image regions (Fujimoto et al., 2009b).

Next, we investigated the bifurcations of out-of-phase periodic points on the (k_r, ϕ)-plane. (Musashi et al., 2009). As shown in Fig. 8(b), their tangent bifurcations and D-type of branchings were found. For example, there are stable out-of-phase m-periodic points in the shaded parameter region surrounded by G_ℓ^m and D_1^m for $m = 30, 32, 34, 36$ for the observed periodic points. Note that the overlapping parameter region indicates that

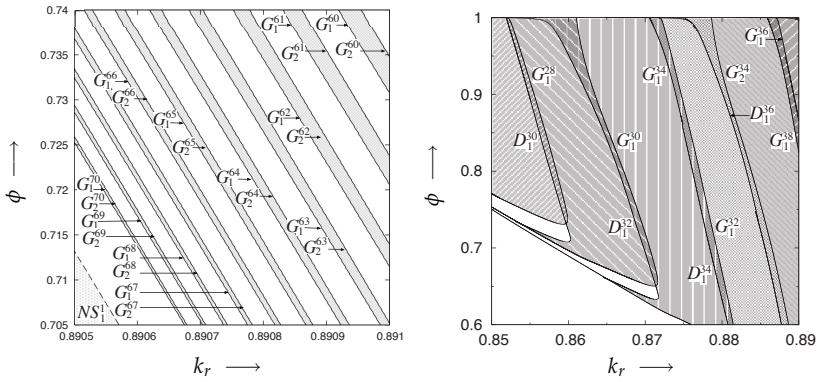

(a) In-phase periodic points (b) Out-of-phase periodic points

Fig. 8. Bifurcations of perodic points observed in symmetric two-coupled system

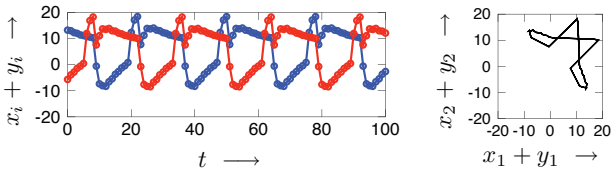

Fig. 9. Out-of-phase oscillatory response observed in asymmetric two-coupled system at $k_r = 0.85$ and $\phi = 0.8$

out-of-phase periodic points coexist. The whole parameter region where there are stable out-of-phase periodic points is much wider than that of stable in-phase periodic points. This is favorable for dynamic image segmentation, because an in-phase periodic point is unsuitable and an out-of-phase periodic point is suitable.

We set $d_1 \neq d_2$ in the two-coupled system, and therefore, the symmetry for the exchange of (x_1, y_1) and (x_2, y_2) in Eq. (6) is lost. This asymmetric two-coupled system corresponds to a situation where an input image contains two image regions of different colors. No symmetric periodic points occur in this system; however, we could observe the asymmetric out-of-phase periodic point shown in Fig. 9. Note that it is difficult to determine whether a periodic point is symmetric only from waveforms and phase portraits; however, this is not important because the feasibility of dynamic image segmentation is not dependent on whether there is symmetry or not but on the number of phases in a periodic point.

Figure 10(a) shows bifurcation sets of out-of-phase periodic points observed at $d_1 = 2$ and $d_2 = 1.9$. Different from the symmetric system, D-type of branching never appeared due to the asymmetric system; instead, period-doubling bifurcations were found. Comparing the extent of all the shaded parameter regions in Figs. 8(b) and 10(a), the asymmetric system is as wide as the symmetric system. Moreover, we set $d_1 = 2$ and $\phi = 0.8$ and investigated their bifurcations on the (k_r, d_2)-plane as seen in Fig. 10(b). This indicates that there were stable out-of-phase periodic points even if the value of $|d_1 - d_2|$ was large; in other words, the

difference between the gray levels of the pixels in the two image regions is large. This is also favorable for a dynamic image segmentation system.

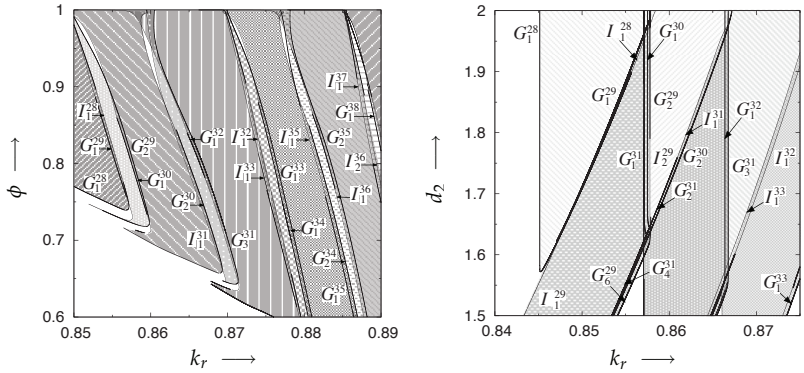

(a) Case of $d_1 = 2$ and $d_2 = 1.9$ (b) Case of $d_1 = 2$ and $\phi = 0.8$

Fig. 10. Bifurcations of out-of-phase perodic points observed in asymmetric two-coupled system

3.3.3 Three-coupled system

This model is composed of a global inhibitor and three neurons without direct coupling to the others and was derived as a reduced model of our dynamic segmentation of an image containing three image regions. As well as the aforementioned reduced models, we drew several two-parameter bifurcation diagrams to find the parameter regions such that a stable fixed point or a stable m-periodic point existed.

When we set $d_1 = d_2 = d_3 = 2$, the three-coupled system was symmetric for a circular exchange of (x_i, y_i) for (x_{i+1}, y_{i+1}), $i = 1, 2, 3$ where the value of $i+1$ returns to 1 if $i = 3$. In this symmetric system, we found a stable fixed point, $\boldsymbol{x}^* = (32.244, -29.167, 32.244, -29.167, 32.244, -29.167, 0.222)$, at $k_r = 0.88$ and $\phi = 0.8$. In the results we investigated, we found the bifurcation diagram on the fixed point on the (k_r, ϕ)-plane was the same as the one in Fig. 5. Moreover, as well as those in the symmetric two-coupled system, we could observe in-phase oscillatory responses in only the right hand side region of NS_1^1. The waveform of an in-phase oscillatory response and its phase portraits are shown in Fig. 11(a), where the blue, red, and green points correspond to the responses of the first, second, and third neurons. The results suggest that the Neimark-Sacker bifurcation set, NS_1^1, causes in-phase oscillatory responses to generate and these are similar to those of the symmetric two-coupled system (Fujimoto et al., 2009b; Musashi et al., 2009). Therefore, this implies that the global bifurcation structure of a fixed point and the generation of in-phase oscillatory responses are intrinsic properties of the symmetric Q-coupled system.

We also observed several oscillatory responses in certain parameter regions. Figures 11(b) and 11(c) show a two-phase and a three-phase periodic points. For the following reasons, we only focused on the bifurcations of three-phase periodic points that were appropriate for dynamically segmenting an image with three image regions.

Figure 13 shows bifurcation sets of three-phase periodic points observed in the symmetric system. Tangent, period-doubling, and Neimark-Sacker bifurcations were observed. The

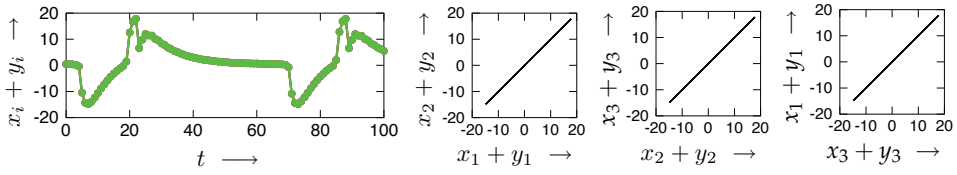

(a) In-phase oscillatory response

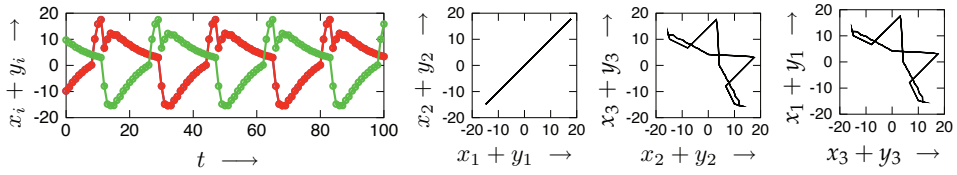

(b) Two-phase oscillatory response

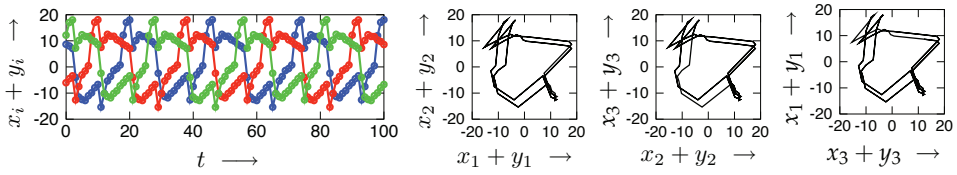

(c) Three-phase oscillatory response

Fig. 11. Different types of oscillatory responses observed in symmetric three-coupled system at $d_1 = d_2 = d_3 = 2$, $k_r = 0.89$, and $\phi = 0.8$

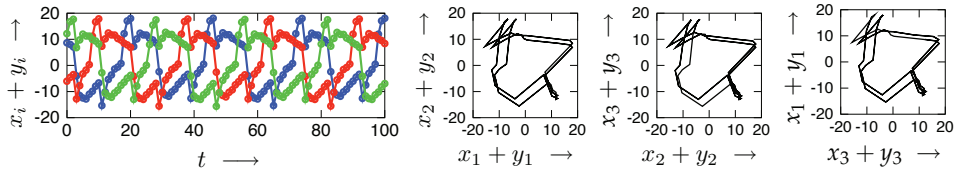

Fig. 12. Three-phase oscillatory response observed in asymmetric three-coupled system at $d_1 = 2$, $d_2 = 1.9$, $d_3 = 1.8$, $k_r = 0.89$, and $\phi = 0.8$

respective periodic points are symmetrical for the aforementioned circular exchange. However, as seen in Fig. 13, we could find no D-type of branching in these investigations. There is a stable three-phase periodic point in each shaded parameter region. Compared with the extent of the entire shaded parameter region in Fig. 8(b), that of the three-phase periodic points is small; however, it is sufficient to design the parameters of our dynamic image segmentation system.

Next, we set $d_1 \neq d_2 \neq d_3$, i.e., this model is asymmetric. Although this three-coupled system loses symmetry, there is a three-phase periodic point in certain parameters as shown in Fig. 12. We investigated the bifurcations of several three-phase periodic points observed in the asymmetric system and drew two bifurcation diagrams. Figure 14(a) shows the bifurcation sets of three-phase periodic points on the (k_r, ϕ)-plane. Of course, we found no D-type of

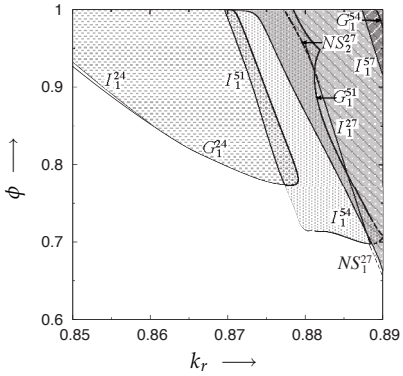

Fig. 13. Bifurcations of three-phase periodic points observed in symmetric three-coupled system

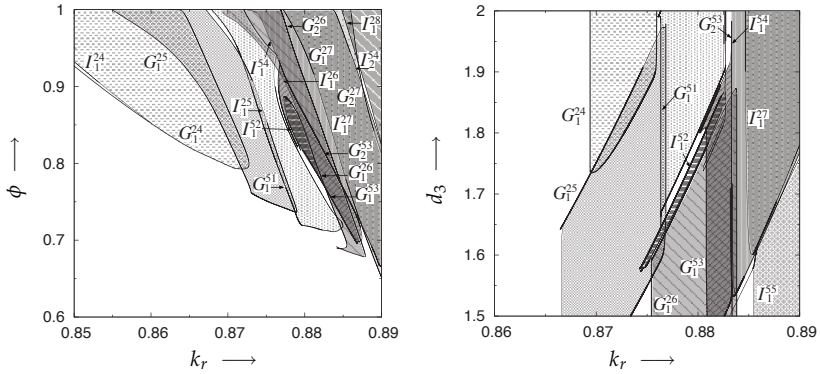

(a) $d_1 = 2$, $d_2 = 1.9$, and $d_3 = 1.8$ (b) $d_1 = 2$, $d_2 = 1.9$, and $\phi = 0.8$

Fig. 14. Bifurcations of three-phase periodic points observed in asymmetric three-coupled system

branching because of the asymmetric system. There is a stable three-phase periodic point in each parameter region shaded by a pattern. The shape and size of the whole shaded parameter region where there are three-phase periodic points are similar to those in Fig. 13.

As seen in Fig. 14(b), we also computed the bifurcations of three-phase periodic points observed at $d_1 = 2$, $d_2 = 1.9$, and $\phi = 0.8$ on the (k_r, d_3)-plane. As we can see from the figure, there are several stable three-phase periodic points even if the value of d_3 is set as small as 1.5. This suggests that our dynamic image-segmentation system can work for an image with three regions having different gray levels.

4. Application to Dynamic Image Segmentation

We demonstrated successful results for dynamic image segmentation carried out by our system with appropriate parameter values according to the results analyzed from the two- and

three-coupled systems. Our basic concept was that we assigned system parameters to certain values such those in-phase oscillatory responses, which are unsuitable for dynamic image segmentation. They do not appear but a multiphase periodic point with as many phases as image regions does occur.

4.1 Image with two image regions

Let us consider a dynamic image segmentation problem for the 8-bit gray-level image with 256×256 pixels shown in Fig. 15(a). This is a slice from the X-ray CT images of the human head from the Visible Human Dataset (Ackerman, 1991). Using a thresholding method, we transformed the gray-level CT image into a binary image in preprocessing with $\forall i, p_i = \{0, 255\}$, where p_i denotes the ith pixel value. Here, the black and white correspond to 0 and 255. The process image contains the two white image regions shown in Fig. 15(b). The upper region corresponds to teeth and the mandible bone, and the lower regions indicate the cervical spine.

We need a neuronal network system to segment the binary image consisting of 256×256 neurons and a global inhibitor. The DC-input value to the ith neuron, d_i, was set to 2.0 for neurons corresponding to pixels in the two white image regions based on $d_i = 2p_i/255$. Therefore, we can design system-parameter values according to the analyzed results for the symmetric two-coupled system in Figs. 5 and 8.

Based on the information in the bifurcation diagrams, we set the two unfixed parameters to $k_r = 0.885$ and $\phi = 0.8$, which correspond to a parameter point in the left neighborhood of NS_1^1 in Fig. 5, so that no in-phase oscillatory responses appear from any initial values but a fixed point or an out-of-phase 36-periodic point does occur. Note that, any of the out-of-phase periodic points in Fig. 8(b) are available for dynamic image segmentation, and the period of the periodic point used in dynamic image segmentation corresponds to the period each segmented image appeared in output images that were exhibited in a time series.

The binarized image was input to our dynamic image segmentation system with 256×256 neurons and a global inhibitor. According to an out-of-phase 36-periodic point, our system output images in the time series shown in Fig. 15(c), i.e., images were dynamically segmented successfully. Note that the output images sequentially appeared from the top-left to the bottom-right, and they also began to appear in each line from the left; moreover, output images corresponding to state variables in the transient state were removed. We confirmed from the series of output images that the period where each image region appeared was 36.

4.2 Image with three image regions

We considered the 8-bit gray-level image with 128×128 pixels shown in Fig. 16(a). It has three image regions: a ring shape, a rectangle, and a triangle. To simplify the problem, the color in each image region was made into a monotone in which the pixel values were 255, 242, and 230 so that these values corresponded to $d_1 = 2$, $d_2 = 1.9$, and $d_3 = 1.8$ according to $d_i = 2p_i/255$. To dynamically segment the target image, we needed a neuronal network system consisting of 128×128 neurons and a global inhibitor. The DC-input value to the ith neuron, d_i, was set to 2.0 for neurons corresponding to pixels in the ring shape, 1.9 for those in the rectangle, and 1.8 for those in the triangle. The neuronal network system with 128×128 neurons could be regarded as an asymmetric three-coupled system. Therefore, according to the analyzed results in Fig. 14, e.g., we set the unfixed parameter values to $k_r = 0.875$ and $\phi = 0.8$ such that a three-phase 25-periodic point occurred in the asymmetric three-coupled system.

(a) CT image (b) Binarization

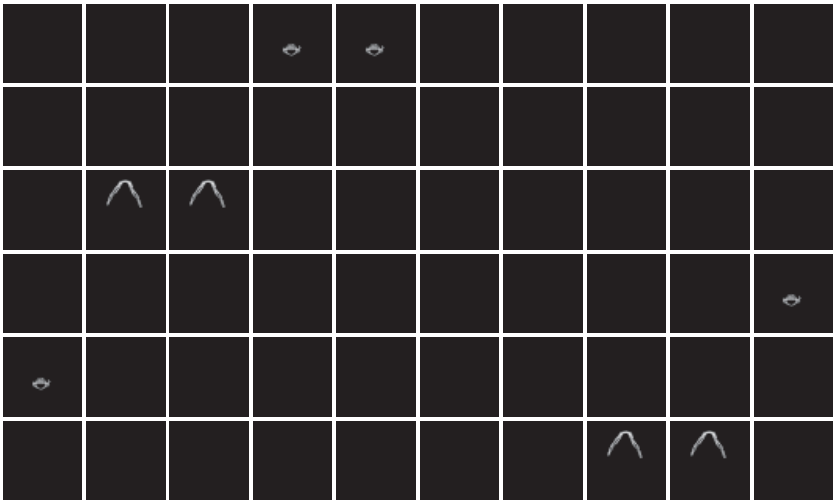

(c) Output images in time series

Fig. 15. Results of dynamic image segmentation based on out-of-phase oscillatory response

In trials for randomly given initial values, we achieved a successful result where three image regions appeared separately, as shown in Fig. 16(b). In addition, because the output images were generated according to a three-phase 25-periodic point observed in the asymmetric three-coupled system, we confirmed that the period where each image region appeared was 25. Note that we removed output images corresponding to state variables in the transient state. Our neuronal network system could work for a simple gray-level image with three image regions.

4.3 Image with many image regions

To segment an image with an arbitrary number of image regions using our dynamic image-segmentation system in one process, it is necessary for a multiphase periodic oscillatory response with as many phases as image regions to appear. As far as our investigations were concerned, however, it was difficult to generate a multiphase periodic point with many phases. Therefore, we proposed an algorithm that successively and partially segments an image.

Here, according to the previously mentioned results obtained from analysis, we considered a successive algorithm that partially segmented many image regions using two- and three-phase oscillatory responses. We let the gray-level image with five image regions in Fig. 17(a) be the target that should be segmented. To simplify the segmentation problem, we

(a) Target image

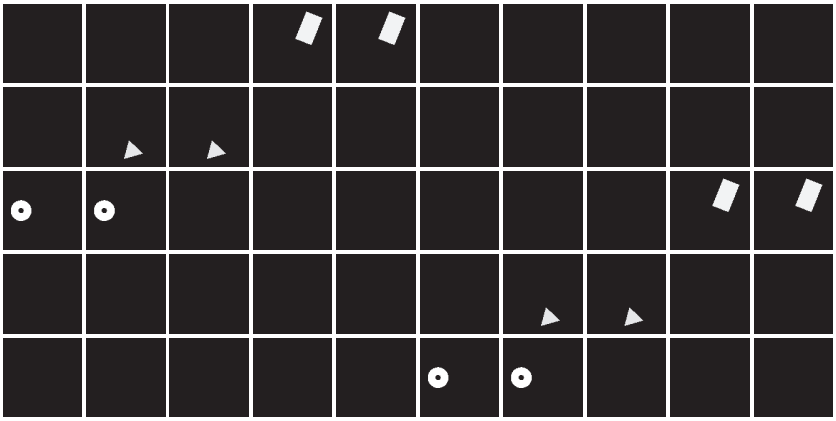

(b) Output images in time series

Fig. 16. Results of dynamic image segmentation based on three-phase oscillatory response

assumed that all pixels in an identical image region would have the same gray levels. Based on the analyzed results for two- and three-coupled systems, we set the system parameters to certain values such that no in-phase oscillatory responses occurred but a fixed point or a two- or three-phase oscillatory responses appeared.

We could obtain the three segmented images in Figs. 17(b)–(d) in the first step from the input image in Fig. 17(a) if a three-phase oscillatory response appeared. Note that the segmented images were extracted from output images in a time series by removing duplicate images and all black images.

Each segmented image in Figs. 17(b)–(d) became an input image for our system in the next step. We obtained the two images in Figs. 17(e) and 17(f) in this step from the input image in Fig. 17(b) using a two-phase oscillatory response; as well as this process, we also obtained the two images in Figs. 17(g) and 17(h) from the input image in Fig. 17(c) according to the two-phase response; whereas we obtained no output images from the input image in Fig. 17(d) because the system to segment the image corresponded to a single neuronal system, and a fixed point always appeared under the system-parameter values we assigned. Therefore, the segmentation of the image in Fig. 17(d) was terminated in this step.

The four images with only one image region in Figs. 17(e)–(h) are input images in the third step. As previously mentioned, we obtained no output images for an input image with only one image region. Therefore, our successive algorithm was terminated at this point in time. Thus, we could segment an image with an arbitrary number of image regions based on the successive algorithm.

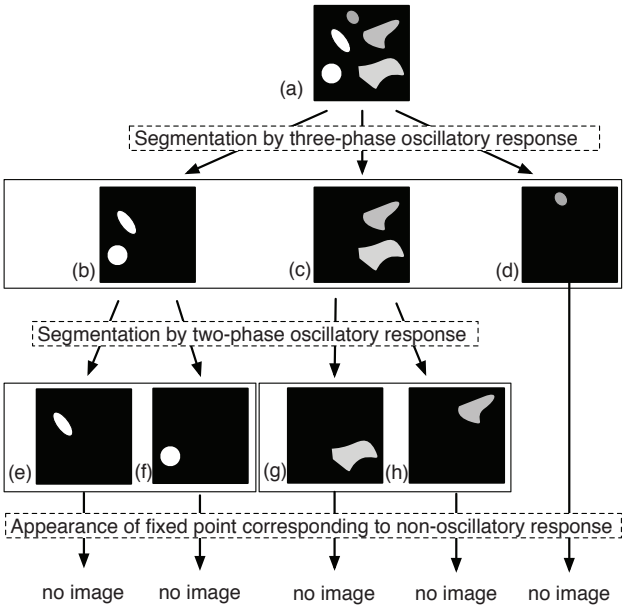

Fig. 17. Schematic diagram of successive algorithm using our dynamic image-segmentation system

5. Concluding remarks

We introduced a discrete-time neuron model that could generate similar oscillatory responses formed by periodic points to oscillations observed in a continuous-time relaxation oscillator model. The scheme of dynamic image segmentation was illustrated using our neuronal network system that consisted of our neurons arranged in a 2D grid and a global inhibitor. Note that we suggested that a neuronal network system where neurons are arranged in a 3D grid can be applied to segmenting a 3D image.

Images were dynamically segmented according to the responses of our system, and therefore, knowing about the bifurcations of the responses allowed us to directly set system-parameter values such that appropriate responses for dynamic image segmentation would appear. We derived reduced models that simplified our analysis of bifurcations observed in our neuronal network system and we found parameter regions where there was a non-oscillatory response or a periodic oscillatory response in the reduced models. According to the analyzed results, we set system parameters to appropriate values, and the designed system could work for two sample images with two or three image regions. Moreover, to segment an image with many image regions, we proposed a successive algorithm using our dynamic image-segmentation system.

We encountered three main problems that should be solved to enable the practical use of our dynamic image-segmentation system:

1. Development of a method that can form appropriate couplings between neurons for a textured image and a gray-level image containing gradation.

2. Development of a method that can give initial values to neurons and a global inhibitor so that an appropriate response will always appear.
3. Development of a method or system that can provide fast processing using our system to segment a large-scale image and a 3D image within practical time limits.

To solve the first problem, we proposed a dynamic image-segmentation system with a method of posterization (Zhao et al., 2003) used as preprocessing (Fujimoto et al., 2009a; 2010). However, their method of posterization involves high computational cost and a large memory, we are considering a neuronal network system with plastic couplings as weight adaptation (Chen et al., 2000). We proposed a solution to the second problem with a method that avoids the appearance of non-oscillatory responses (Fujimoto et al., 2011a). However, toward an ultimate solution, we are investigating parameter regions such that no inappropriate responses appear through bifurcation analysis. An implementation to execute our dynamic image-segmentation system on a graphics processing unit is in progress as a means of rapid processing.

6. Acknowledgments

This study was partially supported by the Ministry of Education, Culture, Sports, Science and Technology, Japan, Grant-in-Aid for Young Scientists (B), Nos. 20700209 and 22700234.

7. References

Ackerman, M. J. (1991). The visible human project, *J. Biocommun.* 18(2): 14.

Aihara, K. (1990). Chaotic neural networks, *in* H. Kawakami (ed.), *Bifurcation Phenomena in Nonlinear Systems and Theory of Dynamical System*, World Scientific, Singapore, pp. 143–161.

Aihara, K., Takabe, T. & Toyoda, M. (1990). Chaotic neural networks, *Phys. Lett. A* 144(6,7): 333–340.

Chen, K., Wang, D. L. & Liu, X. (2000). Weight adaptation and oscillatory correlation for image segmentation, *IEEE Trans. Neural Netw.* 11(5): 1106–1123.

Doi, K. (2007). Computer-aided diagnosis in medical imaging: Historical review, current status and future potential, *Comput. Med. Imaging Graph.* 31(4,5): 198–211.

FitzHugh, R. (1961). Impulses and physiological states in theoretical models of nerve membrane, *Biophys. J.* 1(6): 445–466.

Fujimoto, K., Musashi, M. & Yoshinaga, T. (2008). Discrete-time dynamic image segmentation system, *Electron. Lett.* 44(12): 727–729.

Fujimoto, K., Musashi, M. & Yoshinaga, T. (2009a). Dynamic image segmentation system for ultrasonic B-mode image based on its multi-scaled feature maps, *Proc. 2009 Int. Symposium on Nonlinear Theory and its Applications*, IEICE, Japan, Sapporo, pp. 495–498.

Fujimoto, K., Musashi, M. & Yoshinaga, T. (2009b). Reduced model of discrete-time dynamic image segmentation system and its bifurcation analysis, *Int. J. Imaging Syst. Technol.* 19(4): 283–289.

Fujimoto, K., Musashi, M. & Yoshinaga, T. (2010). Dynamic image segmentation system with multi-scaling system for gray scale image, *Proc. the Third Int. Conf. on Bio-inspired Systems and Signal Processing*, INSTICC Press, Valencia, pp. 159–162.

Fujimoto, K., Musashi, M. & Yoshinaga, T. (2011a). Discrete-time dynamic image segmentation based on oscillations by destabilizing a fixed point, *IEEJ Trans. Electr. Electron. Eng.* 6(5). (to appear).

Fujimoto, K., Musashi, M. & Yoshinaga, T. (2011b). FPGA implementation of discrete-time neuronal network for dynamic image segmentation, *IEEJ Trans. Electronics, Infomation and Systems* 131(3). (to appear).

Haschke, R. & Steil, J. J. (2005). Input space bifurcation manifolds of recurrent neural networks, *Neurocomputing* 64: 25–38.

Hodgkin, A. L. & Huxley, A. F. (1952). A quantitative description of membrane current and its application to conduction and excitation in nerve, *J. Physiol.* 117(4): 500–544.

Kapral, R. (1985). Pattern formation in two-dimensional arrays of coupled, discrete-time oscillators, *Phys. Rev. A* 31(6): 3868–3879.

Kawakami, H. (1984). Bifurcation of periodic responses in forced dynamic nonlinear circuits: computation of bifurcation values of the system parameters, *IEEE Trans. Circuits Syst.* 31(3): 248–260.

Musashi, M., Fujimoto, K. & Yoshinaga, T. (2009). Bifurcation phenomena of periodic points with high order of period observed in discrete-time two-coupled chaotic neurons, *J. Signal Processing* 13(4): 311–314.

Oppo, G.-L. & Kapral, R. (1986). Discrete models for the formation and evolution of spatial structure in dissipative systems, *Phys. Rev. A* 33(6): 4219–4231.

Pal, N. R. & Pal, S. K. (1993). A review on image segmentation techniques, *Pattern Recognit.* 26(9): 1277–1294.

Pikovsky, A., Rosenblum, M. & Kurths, J. (2003). *Synchronization: A universal concept in nonlinear sciences*, Cambridge University Press, Cambridge.

Rulkov, N. F. (2002). Modeling of spiking-bursting neural behavior using two-dimensional map, *Phys. Rev. E* 65(4): 041922.

Shareef, N., Wang, D. L. & Yagel, R. (1999). Segmentation of medical images using legion, *IEEE Trans. Med. Imaging* 18(1): 74–91.

Suri, J. S., Wilson, D. L. & Laxminarayan, S. (2005). *Handbook of Biomedical Image Analysis*, Kluwer Academic / Plenum Publishers, New York.

Terman, D. & Wang, D. L. (1995). Global competition and local cooperation in a network of neural oscillators, *Physica D* 81(1,2): 148–176.

Waller, I. & Kapral, R. (1984). Spatial and temporal structure in systems of coupled nonlinear oscillators, *Phys. Rev. A* 30(4): 2047–2055.

Wang, D. L. (2005). The time dimension for scene analysis, *IEEE Trans. Neural Netw.* 16(6): 1401–1426.

Wang, D. L. & Terman, D. (1995). Locally excitatory globally inhibitory oscillator networks, *IEEE Trans. Neural Netw.* 6(1): 283–286.

Wang, D. L. & Terman, D. (1997). Image segmentation based on oscillatory correlation, *Neural Comput.* 9(4): 805–836.

Zhao, L., Furukawa, R. A. & Carvalho, A. C. (2003). A network of coupled chaotic maps for adaptive multi-scale image segmentation, *Int. J. Neural Syst.* 13(2): 129–137.